My own beliefs are that the road to a scientific discovery is seldom direct, and it does not necessarily require great expertise. In fact, I am convinced that often a newcomer to a field has a great advantage because he is ignorant and does not know all the reasons why a particular experiment should not be attempted.—*Ivan Giaever (discoverer of tunnelling between superconductors), Nobel prize address, 1973*

CHAPTER 10

Superconductivity

10.1 INTRODUCTION

Superconductivity was discovered by H. Kamerlingh Onnes in 1911, three years after his first liquefaction of helium. The availability of this liquid enabled him to investigate the electrical resistance of metals at low temperatues. He chose mercury for study since it could be readily purified by distillation and there was speculation at that time that the resistance of very pure metals might tend to zero at $T = 0$. As can be seen from Fig. 10.1, the observed behaviour was much more dramatic than this; an abrupt transition to a state of apparently zero resistance occurs at a temperature of about 4.2 K. Onnes described the new state as the superconducting state, and it was quickly established that there was no essential connection with high purity; adding substantial amounts of impurity often has little effect on the superconducting transition, although the resistance of the normal state (section 3.3.2) is increased considerably.

Subsequently many metals and alloys have been shown to become superconducting.† The superconducting transition can be very sharp, with a width of less than 10^{-3} K in well annealed single crystals of a metal such as tin. The element with the highest transition temperature, $T_c = 9.2$ K, is niobium (Nb). The search

† Among common metallic elements that *do not* become superconducting at temperatures currently accessible are copper, silver, gold, the alkali metals and magnetically ordered metals such as iron, nickel and cobalt.

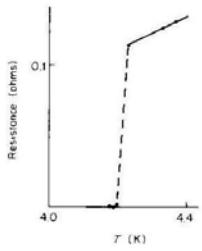

Fig. 10.1 Superconducting transition of mercury. (After H. Kamerlingh Onnes, *Leiden Commun.* **124c** (1911))

for materials with higher transition temperatures led to the investigation of alloys and compounds. In 1972 Nb_3Ge was found to have a T_c of 23 K. For the next 14 years this remained the record T_c and many researchers were misled, with some theoretical justification, into believing that it would not be possible to find materials with significantly higher transition temperatures. In 1986 there was a dramatic breakthrough when Bednorz and Muller found that $La_{2-x}Ba_xCuO_4$ had a T_c of about 35 K for $x \approx 0.15$. This discovery was followed by a frenetic search for other materials. In 1987 $YBa_2Cu_3O_{7-\delta}$ ($\delta \approx 0.1$) was found to have a T_c of 92 K and in 1988 $Bi_2Sr_{3-x}Ca_xCu_2O_{8+\delta}$ ($x \leqslant 1$) raised T_c to 110 K. At the time at which this book was written $Tl_2Ba_2Ca_2Cu_3O_{10}$, also discovered in 1988, has the highest known T_c of 125 K. These new **high-temperature superconductors** are discussed further in section 10.6.

No one has succeeded in measuring a finite resistance to small currents in the superconducting state. The most sensitive method for detecting a small resistance is to look for the decay of a current around a closed superconducting loop. If the resistance of the loop is R and the self-inductance L then the current should decay with time constant $\tau = L/R$. Failure to observe the decay of a **persistent current** has enabled an upper limit of about $10^{-26}\ \Omega$ m to be put on the resistivity of superconductors as compared to a value of order $10^{-8}\ \Omega$ m for copper at room temperature (problem 10.1).

10.2 MAGNETIC PROPERTIES OF SUPERCONDUCTORS

10.2.1 Type I superconductors

Superconductors divide into two classes according to their behaviour in a magnetic field. In this section we describe the simpler behaviour of **type I**

superconductors and in section 10.2.3 that of **type II superconductors**. All pure samples of superconducting elements, except Nb, exhibit type I behaviour and their superconductivity is destroyed by a modest applied magnetic field B_c, known as the **critical field**. B_c is shown as a function of temperature for mercury in Fig. 10.2. To a good approximation the temperature dependence of B_c is

$$B_c(T) \approx B_c(0)\left[1 - \left(\frac{T}{T_c}\right)^2\right]. \qquad (10.1)$$

It follows from the existence of a critical field that there will be a critical current for flow along a wire, which occurs when the field due to the current equals B_c; this is known as the **Silsbee hypothesis**.

In 1933, Meissner and Ochsenfeld investigated the variation in space of the magnetic field in the neighbourhood of a superconductor and discovered that the field distribution was consistent with the field inside the superconductor being zero. This exclusion of the magnetic flux from the superconductor is known as the **Meissner effect** and is due to electric currents, known as **screening** currents, flowing on the surface of the superconductor in such a way as to generate a field equal and opposite to the applied field. The expulsion of the flux when the field is reduced below B_c at constant temperature is illustrated in Fig. 10.3 for a sample in the form of a long cylinder; expulsion also occurs if the sample is cooled into the superconducting state in a steady applied field. For many purposes we can take account of the Meissner effect by regarding the superconductor as a magnetic material in which the screening currents are replaced by an equivalent magnetization; since we require $\mathbf{B} = \mu_0(\mathbf{H} + \mathbf{M}) = 0$ we must have

$$\mathbf{M} = -\mathbf{H}. \qquad (10.2)$$

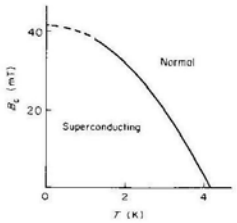

Fig. 10.2 Critical field curve of mercury

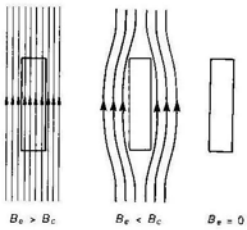

Fig. 10.3 Expulsion of flux by a long superconducting cylinder when the field is reduced below B_c. In equilibrium there is no trapped flux

Comparison of Eq. (10.2) with Eq. (7.1) shows that a type I superconductor behaves as though it has a magnetic susceptibility $\chi = -1$ and is consequently often referred to as a **perfect diamagnet**. Fig. 10.4 illustrates how closely a well annealed long cylinder of lead conforms to the behaviour predicted by Eq. (10.2).

Non-annealed specimens often show an incomplete Meissner effect; magnetic flux is trapped within the material in metastable regions which remain the normal state when the field is reduced through B_c. Flux trapping offers a partial explanation of the 22 year delay between the first observation of superconductivity and the discovery of the Meissner effect. It was not realized that the trapped flux was only a manifestation of non-equilibrium behaviour; instead it was regarded as an inevitable consequence of the infinite conductivity of the

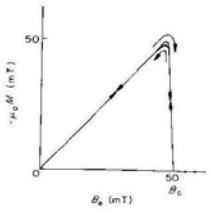

Fig. 10.4 Almost reversible magnetization curve of a well annealed rod of pure superconducting lead. (Reproduced with permission from J. P. Livingston, *Phys. Rev.* **129**, 1943 (1963))

superconducting state because of the following argument. Infinite conductivity implies vanishing of the electric field inside a superconductor and hence through Faraday's law, curl $\mathbf{E} = -\dot{\mathbf{B}}$, it indicates a time-independent magnetic field. This was erroneously interpreted as implying that any magnetic field within a sample would be trapped by a transition to the superconducting state. The discovery of the Meissner effect showed that the zero flux state was the true equilibrium state of a long cylindrical sample at all fields below B_c.

For other shapes of sample the complete exclusion of flux, even in well annealed specimens, does not occur at all fields less than B_c. To explain this, consider the spherical sample in Fig. 10.5. Because the flux is expelled from the interior of the sphere the field at the equator exceeds the applied field. Thus, when the applied field reaches the value $\frac{2}{3}B_c$, the field at the equator becomes B_c and the sphere can no longer remain in the Meissner state. It cannot make a transition to the normal state because this would reduce the field everywhere to $\frac{2}{3}B_c$, a value at which the normal state is not stable. For applied fields between $\frac{2}{3}B_c$ and B_c the sphere is in the **intermediate state** in which it consists of alternating *macroscopic* normal and superconducting regions, shown schematically in Fig. 10.5(*b*); the field is B_c in the normal regions and zero in the superconducting regions. The intermediate state of a type I superconductor should not be confused with the mixed state of a type II superconductor (sections 10.2.3 and 10.5.3).

The existence of the critical field B_c is a consequence of the Meissner effect. The energy stored in the field ($B^2/2\mu_0$ per unit volume) is greater for the Meissner state than for the normal state in which the field penetrates the

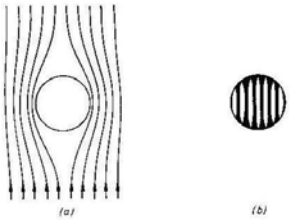

Fig. 10.5 (*a*) Superconducting sphere in the Meissner state. The field at the equator is 50% higher than the applied field. (*b*) Intermediate state of a type I superconducting sphere, appropriate to applied fields between $\frac{2}{3}B_c$ and B_c. With increasing field in this range the shaded normal regions grow at the expense of the unshaded superconducting regions. For simplicity the field lines are not shown

material uniformly† (we can usually ignore the weak magnetism of the normal state). Eventually, with increasing magnetic field, the increased magnetic field energy equals the energy difference between the normal and superconducting states and it becomes advantageous for the material to make a transition to the normal state. To quantify this argument we must do some simple thermodynamics

10.2.2. Thermodynamics of the superconducting transition

The field B_c at which the normal (N) and superconducting (S) states are in equilibrium is indicated by the equality of their Gibbs free energies. We take the magnetic work term to be $-\mathbf{M}.\mathrm{d}\mathbf{B}_e$, where $\mathbf{B}_e$ is the applied field, and the Gibbs free energy per unit volume is then‡

$$G = U - TS$$

where U and S are the internal energy and entropy per unit volume. To see this we calculate

$$\begin{aligned} \mathrm{d}G &= \mathrm{d}U - T\,\mathrm{d}S - S\,\mathrm{d}T = T\,\mathrm{d}S - \mathbf{M}.\mathrm{d}\mathbf{B}_e - T\,\mathrm{d}S - S\,\mathrm{d}T \\ &= -\mathbf{M}.\mathrm{d}\mathbf{B}_e - S\,\mathrm{d}T. \end{aligned} \tag{10.3}$$

Thus G is the thermodynamic function that is minimized in thermal equilibrium at fixed temperature and applied field.

Consider a long cylinder of superconductor parallel to the applied field. Eq. (10.3) can be integrated at constant temperature to deduce the effect of an applied field on the free energy G_S of a superconductor,

$$G_S(B_e, T) = G_S(0, T) - \int_0^{B_e} \mathbf{M}.\mathrm{d}\mathbf{B}_e. \tag{10.4}$$

For a long cylinder we show in appendix B that $\mathbf{B}_e = \mu_0\mathbf{H}$, where $\mathbf{H}$ is the field inside the superconductor. Inserting $\mathbf{M} = -\mathbf{H}$ (Eq. (10.2)) for a superconductor in its Meissner state, we obtain

$$G_S(B_e, T) = G_S(0, T) + \int_0^{B_e} \frac{B_e}{\mu_0}\,\mathrm{d}B_e = G_S(0, T) + \frac{B_e^2}{2\mu_0}. \tag{10.5}$$

† The magnetic energy *inside* the material is smaller for the Meissner state because $B = 0$ there, but the increased energy outside more than compensates.

‡ See Mandl[2] for a discussion of magnetic work. It is more common in superconductivity, although not in magnetism, to take the work term to be $+\mathbf{B}_e.\mathrm{d}\mathbf{M}$, appropriate to an internal energy, $U' = U + \mathbf{M}.\mathbf{B}_e$, which includes the energy of interaction, $+\mathbf{M}.\mathbf{B}_e$, of the specimen with the sources of the external field. In this approach G is written $G = U' - TS - \mathbf{M}.\mathbf{B}_e$. By not including a term PV in G we are ignoring the effect of changes in pressure and volume on the superconducting transition.

where the final term represents the additional magnetic energy associated with the exclusion of the magnetic field, as discussed at the end of the previous section. If we ignore the weak magnetism of the normal state then the Gibbs free energy G_N of this state is field-independent,

$$G_N(B_e, T) = G_N(0, T).$$

Equating the Gibbs free energies at the critical field then gives

$$G_N(0, T) - G_S(0, T) = \frac{B_c^2}{2\mu_0} \tag{10.6}$$

so that the critical field is directly related to the difference in free energies between the normal and superconducting states in zero field; for this reason B_c is often referred to as the thermodynamic critical field. The positive value of $G_N - G_S$ explains why the superconducting state is more stable than the normal state in zero field; this quantity is the **condensation energy** of the superconducting state.

Experimentally it is found approximately that $B_c \propto T_c$ with a constant of proportionality of order 0.01 T K^{-1}; thus, from Eq. (10.6), the condensation energy is of order $40T_c^2$ J m^{-3}. This energy difference corresponds to a fraction $k_B T_c/\varepsilon_F$ of the conduction electrons having their energy reduced by an amount $k_B T_c$ as result of the transition to superconductivity, and is therefore smaller by a factor $(k_B T_c/\varepsilon_F)^2 \sim 10^{-7}$ than the total kinetic energy of the electrons.

Two important exact results for type I superconductors can be obtained from Eq. (10.6). Using $S = -(\partial G/\partial T)$ (from Eq. (10.3)) we find that the difference in entropy density between the two states in zero field is

$$\Delta S = S_S - S_N = \frac{1}{2\mu_0}\frac{\mathrm{d}B_c^2}{\mathrm{d}T} = \frac{B_c}{\mu_0}\frac{\mathrm{d}B_c}{\mathrm{d}T}, \tag{10.7}$$

and using $C = T\partial S/\partial T$, the difference in heat capacity per unit volume in zero field is

$$\Delta C = C_S - C_N = \frac{T}{2\mu_0}\frac{\mathrm{d}^2 B_c^2}{\mathrm{d}T^2} = \frac{T}{\mu_0}\left[B_c\frac{\mathrm{d}^2 B_c}{\mathrm{d}T^2} + \left(\frac{\mathrm{d}B_c}{\mathrm{d}T}\right)^2\right]. \tag{10.8}$$

Using Eqs. (10.7) and (10.8) in conjunction with a critical field curve of the form shown in Fig. 10.2 enables us to make some important qualitative deductions:

(1) The entropy difference ΔS vanishes at T_c since $B_c = 0$ there, but the heat capacity difference ΔC is finite since $\mathrm{d}B_c/\mathrm{d}T > 0$; the discontinuity of the specific heat at T_c is clearly seen in Fig. 10.6, which shows the measured heat capacity of aluminium. The superconducting transition in zero applied field is therefore a second-order phase transition.

(2) ΔS and ΔC vanish at $T = 0$ in accordance with the third law of thermodynamics.

(3) For $0 < T < T_c$, $\mathrm{d}B_c/\mathrm{d}T$ is negative so that $\Delta S < 0$; the superconducting

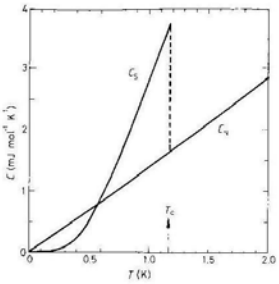

Fig. 10.6 Heat capacity of normal and superconducting aluminium. The normal state measurements were made by applying a field greater than B_c. The high Debye temperature of aluminium means that the lattice contribution to the heat capacity is small in this temperature range and the electronic contribution is dominant. Note the discontinuity in heat capacity at T_c and the exponential fall-off in C_S at low temperature. (After N. E. Phillips, *Phys. Rev.* **114**, 676 (1959))

state is therefore more ordered than the normal state. We discuss the nature of the ordering in section 10.4.

(4) Because ΔS is finite for $0 < T < T_c$ there is a latent heat at the superconducting transition in a finite field given by $T\Delta S$; strictly Eq. (10.7) gives the entropy difference in zero field but ΔS is field-independent. S_N is field-independent because normal state magnetism is very weak and S_S is field-independent because the Meissner effect means that the interior of the superconductor remains in zero field up to B_c.

Deductions (1), (2) and (3) remain valid for a type II superconductor but they must be proved by a different method, as type II superconductors do not exhibit a sharp transition from the Meissner state to the normal state at a field B_c.

10.2.3 Type II superconductors

Although Nb is the only element that is type II in its pure state, other elements generally become type II when the electron mean free path is reduced sufficiently by alloying. Fig. 10.7 compares the magnetization curves of thin cylinders of pure Pb and a Pb–In alloy; with increasing field the alloy shows a complete Meissner effect only up to a field B_{c1} that is less than the thermodynamic critical field of pure Pb. Above B_{c1} there is partial flux penetration into the alloy although it retains the ability, characteristic of the superconducting state, to support dissipationless current flow.† The transition to the normal state and

† The critical current I_c is *not* related to a critical field by the Silsbee hypothesis but depends on the metallurgical state: the more inhomogeneous the material, the higher I_c (see section 10.5.3 for an explanation).

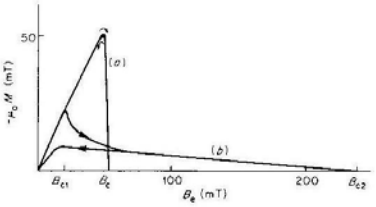

Fig. 10.7 Almost reversible magnetization curves for well annealed long rods of: (*a*) pure lead (as in Fig. 10.4); (*b*) lead made type II by alloying with 8.23% indium. (Reproduced with permission from J. P Livingston, *Phys. Rev.* **129**, 1943 (1963))

complete flux penetration occur at the substantially higher field B_{c2}. Between its **lower** and **upper critical fields**, B_{c1} and B_{c2}, the alloy is in the **mixed state**, the nature of which will be explained in section 10.5.3.

According to Eq. (10.4) the increase in Gibbs free energy associated with the exclusion of magnetic flux by a superconductor is equal to the area, $\int(-\mathbf{M}).d\mathbf{B}_e$, under the magnetization curve. This equation is strictly applicable only to equilibrium states, characterized by reversible magnetization curves. We can however apply it approximately to the almost reversible curve for the Pb–In alloy in Fig. 10.7. The area under this curve is almost equal to that under the curve for pure Pb; we deduce that alloying produces no substantial change in the condensation energy. The partial flux penetration in the mixed state allows the superconductivity to persist to significantly higher fields in the alloy. With increasing indium concentration B_{c1} decreases and B_{c2} increases.

In extreme type II superconductors B_{c1} is so small and the flux penetration in the mixed state so nearly complete that very large values of B_{c2} are reached before the area under the magnetization curve becomes equal to the condensation energy. For large B_{c2} our thermodynamic approach must be generalized to allow for the decrease in Gibbs free energy associated with the weak paramagnetism of the normal state. This decrease puts a fundamental upper limit on B_{c2}, the **Clogston limit**, of about $1.8T_c$ tesla (see problem 10.4). Fig. 10.8 shows values of B_{c2} as a function of temperature for some extreme type II superconductors.

10.3 THE LONDON EQUATION

We saw in section 7.3.2 that the rigidity of an electron wavefunction against perturbation by a magnetic field led directly to diamagnetism with the field being excluded from the region occupied by the electron except for a surface

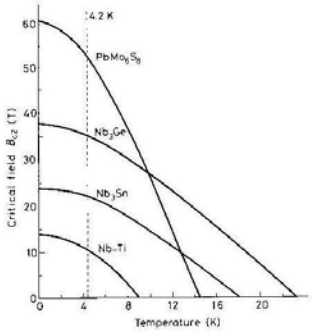

Fig. 10.8 Upper critical field, B_{c2}, as a function of temperature for some extreme type II superconductors. (Reproduced with permission from R. Chevrel, *Superconductor Materials Science: Fabrication and Applications*, ed. S. Foner and B. Schwartz, Plenum, New York (1980))

layer about 100 Å thick. The weakness of diamagnetic effects in most materials is then explained because ordinary *atomic* wavefunctions are small in extent compared to this screening distance. The perfect diamagnetism of superconductors implies that there are wavefunctions extending *throughout* the material that are not readily perturbed by a magnetic field.

This possibility was first suggested by Fritz London, who proposed that the currents responsible for the screening should be described by

$$\text{curl}\,\mathbf{j} = -\frac{n_s e^2}{m}\mathbf{B}. \tag{10.9}$$

Eq. (10.9) is known as the **London equation** and it is the curl of

$$\mathbf{j} = -\frac{n_s e^2}{m}\mathbf{A}, \tag{10.10}$$

which is Eq. (7.32) with the replacement $n \to n_s$ to allow for the possibility that only a fraction n_s/n of the electrons (the **superconducting fraction**) have a rigid wavefunction. Eq. (10.9) (or its equivalent, Eq. (10.10)) can be regarded as a replacement for Ohm's law, $\mathbf{j} = \sigma\mathbf{E}$, as a description of the behaviour of the superconducting electrons.

To see that Eq. (10.9) explains the Meissner effect we apply it to a plane boundary ($x = 0$) separating a superconductor ($x > 0$) from a vacuum ($x < 0$), when there is a magnetic field $\mathbf{B} = B_e\hat{\mathbf{z}}$ parallel to the boundary in the vacuum

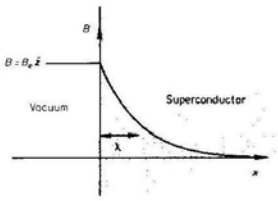

Fig. 10.9 The London equation predicts the exponential decay of a magnetic field into a superconductor occupying the region $x > 0$

(Fig. 10.9). By combining Eq. (10.9) with Maxwell's equations† curl $\mathbf{B} = \mu_0\mathbf{j}$ and div $\mathbf{B} = 0$, we find that the field $\mathbf{B}$ inside a superconductor satisfies

$$\lambda^2\nabla^2\mathbf{B} = \mathbf{B} \tag{10.11}$$

where $\lambda^2 = m/\mu_0 n_s e^2$ as in section 7.3.2. The magnetic field in the superconductor in the geometry of Fig. 10.9 is therefore of the form $\mathbf{B} = B(x)\hat{\mathbf{z}}$, where $B(x)$ satisfies

$$\lambda^2\frac{d^2B}{dx^2} = B.$$

The solution of this equation is

$$B(x) = a\,e^{-x/\lambda} + b\,e^{+x/\lambda}, \tag{10.12}$$

where a and b are constants of integration. The second term, which has B increasing exponentially with x at large distances from the boundary, is unphysical and we reject it. To satisfy $B = B_e$ at $x = 0$ then requires $a = B_e$ so that

$$B(x) = B_e\,e^{-x/\lambda}. \tag{10.13}$$

The magnetic field thus decays exponentially with distance into the superconductor with a characteristic length scale λ, kown as the **penetration depth**, as shown in Fig. 10.9. To estimate λ at $T = 0$ we suppose that all the electrons are superconducting at this temperature and set $n_s = n = 10^{29}\,\text{m}^{-3}$, a typical conduction electron concentration in a superconducting metal, to obtain

$$\lambda = \lambda_L(0) = \left(\frac{m}{\mu_0 ne^2}\right)^{1/2} \approx 170\,\text{Å} \tag{10.14}$$

† It is important to note that in this section we take the screening currents explicitly into account rather than replacing them by their equivalent magnetization. In this approach, which is more appropriate when investigating the behaviour of superconductors at a microscopic level, we put $\mathbf{M} = 0$ and $\mathbf{B} = \mu_0\mathbf{H}$.

where the notation $\lambda_L(0)$ indicates that this is the penetration depth as predicted by the London equation at $T = 0$. The small size of λ means that the magnetic flux is effectively excluded from the interior of macroscopic samples of superconductors and the Meissner effect is explained. Note that in the geometry of Fig., 10.9 the screening currents flow in the y direction and also decay exponentially with characteristic depth λ from the surface of the superconductor.

At higher temperatures we expect n_s to decrease and λ to increase. This is seen to be the case in Fig. 10.10, which shows the measured temperature dependence of λ for tin. The temperature dependence is often well described by

$$\lambda = \frac{\lambda(0)}{[1-(T/T_c)^4]^{1/2}}$$

where $\lambda(0)$ is the value of λ at $T = 0$; λ thus diverges as $T \to T_c$ and $n_s \to 0$.

The measured value of $\lambda(0)$ is often greater than $\lambda_L(0)$. This does not signify a fundamental defect of the London theory; the discrepancy can be explained by modifying Eq. (10.10) slightly so that the current density $\mathbf{j}$ at a point $\mathbf{r}$ does not depend only on the vector potential $\mathbf{A}$ at $\mathbf{r}$ but on the average of $\mathbf{A}$ taken over all points in the neighbourhood of $\mathbf{r}$. This modification converts the **local** current–field relation of Eq. (10.10) into a **non-local relation**. A similar change has to be made to Ohm's law in normal metals when the electric field varies rapidly on the length scale of the electron mean free path l. Such a situation occurs in pure normal metals at high frequencies and low temperature where the electromagnetic skin depth (which gives the length scale for variation of $\mathbf{E}$) is normally shorter than l, and the current density at a point $\mathbf{r}$ then depends on the average of the electric field over a region of size $\sim l$ surrounding $\mathbf{r}$; the necessary generalization of Ohm's law is a non-local relation between $\mathbf{j}$ and $\mathbf{E}$. Pippard exploited the analogy with the normal state to propose that the penetration depth of pure superconductors could be explained if there was a non-local

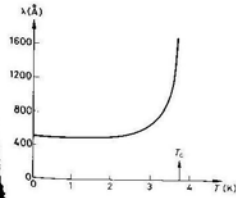

Fig. 10.10 Superconducting penetration depth λ in tin. The value at $T = 0$ is 510 Å, which has to be compared with the London prediction $\lambda_L(0) = 340$ Å

relation between **j** and **A**† in which the vector potential was averaged over a distance ξ, where

$$\xi \approx \frac{\hbar v_F}{k_B T_c} \qquad (\xi \approx 10^4 \text{ Å for } v_F = 10^6 \text{ m s}^{-1} \text{ and } T_c = 10 \text{ K}). \quad (10.15)$$

We show later (section 10.4) that a characteristic distance of this form arises naturally in the theory of superconductivity. In impure superconducting metals where l is less than ξ, the mean free path takes over from ξ in determining the range of the non-locality and λ then depends on l. Pippard's proposals were later confirmed in essence by the microscopic theory of superconductivity.

It is interesting to investigate the extent to which the London equation can be deduced from an assumption of infinite conductivity; to do so we allow the electron scattering time τ in Eq. (3.23) to become infinite. The resulting acceleration equation

$$m_e \, d\mathbf{v}/dt = -e\mathbf{E}$$

together with $\mathbf{j} = -n_s e\mathbf{v}$ and Faraday's law, $\text{curl}\,\mathbf{E} = -\dot{\mathbf{B}}$, lead to the time derivative of Eq. (10.9). To obtain the London equation by integration of this equation involves making an assumption about the integration constant, which is equivalent to assuming the Meissner effect. This again demonstrates that superconductivity is more than just infinite conductivity.

10.4 THE THEORY OF SUPERCONDUCTIVITY

We will give only a brief qualitative description of the very successful microscopic theory of superconductivity that was proposed by Bardeen, Cooper and Schrieffer (BCS) in 1957; the quantitative details of the BCS theory involve techniques that are too advanced for this book.‡

10.4.1 The energy gap and electron pairing

We saw in the previous section that the temperature dependence of the penetration depth suggests a density n_s of superconducting electrons that increased from zero at T_c to the full electron density at $T = 0$. The behaviour is consistent with the existence of an energy gap Δ separating the states of the superconducting electrons from those of the 'normal' electrons. There is a considerable amount of evidence for such a gap; both experiment and theory indicate that Δ is temperature-dependent, vanishing at T_c and attaining its

† Note that high frequencies are not required to cause **A** to vary rapidly in space in a superconductor; even for a dc field, the Meissner effect ensures that **A** varies on a length scale λ.

‡ For an excellent series of review articles on superconductivity the reader is recommended to consult *Superconductivity*, ed. R. D. Parks, Marcel Dekker, New York (1969).

maximum value $\Delta(0)$ at $T = 0$. At low temperatures ($T \ll T_c$) one would expect that the number of excited (normal) electrons would fall off as $\exp[-\Delta(0)/k_B T]$ and that this temperature dependence would be reflected in the electronic contribution to the heat capacity; this is indeed found to be the case (see Fig. 10.6) and $\Delta(0)$ turns out to be of order $k_B T_c$.

Direct evidence for an energy gap is provided by measurements of the absorption of electromagnetic waves. At low temperature ($T \ll T_c$) the absorption is vanishingly small at low frequencies but increases sharply when the photon energy is sufficient to excite electrons across the energy gap. The frequency for the onset of absorption is given by

$$h\nu = 2\Delta(0). \quad (10.16)$$

The factor 2 arises because absorption of a photon creates two excited electrons. A natural explanation for this is provided by the BCS theory of superconductivity, according to which the superconducting electrons are bound together in pairs, known as **Cooper pairs**. Thus 2Δ is the binding energy of a Cooper pair so that Eq. (10.16) describes the breaking of a pair by absorption of a photon. The attractive interaction that binds the pairs is due to the lattice vibrations (section 10.4.3).

The wavefunction of all the pairs has to be identical to maximize the energy reduction due to the attractive interaction; the binding energy of a Cooper pair is largest when all the pairs are in the same state. Superconductivity is therefore said to be a **cooperative phenomenon**; ferromagnetism is another example of a cooperative phenomenon since the better the alignment of the spins, the greater the molecular field that is responsible for the alignment (see section 8.3.1). The existence of a common wavefunction for the Cooper pairs provides the rigidity of the wavefunction that leads to the Meissner effect and it is also responsible for the infinite conductivity (section 10.4.5).

At $T = 0$ all the electrons are paired but at $T > 0$ some pairs are broken by thermal excitation. Because of the cooperative nature of superconductivity, the binding energy of the remaining pairs falls. The resulting decrease in the measured energy gap can be seen in Fig. 10.11; $\Delta(T)$ falls to zero with infinite slope at $T = T_c$. The sharing of a common wavefunction by the pairs is present at all temperatures below T_c and the resulting order is responsible for the lower entropy of the superconducting state.

The average distance between the electrons for the Cooper pair wavefunction in a pure metal at $T = 0$ is of order

$$\xi_0 = \hbar v_F / \pi\Delta(0); \quad (10.17)$$

ξ_0 is known as the **BCS coherence length** and it plays an important role in the theory of superconductivity. Since $\Delta(0) \approx k_B T_c$ (the BCS theory predicts $\Delta(0) = 1.76 k_B T_c$), it is essentially ξ_0 that determines the range of non-locality (Eq. (10.15)) in the current-field relation of the superconducting electrons in a pure

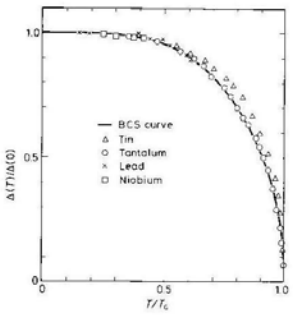

Fig. 10.11 Temperature dependence of the superconducting energy gap. The full curve is the BCS theory prediction. (Reproduced with permission from P. Townsend and J. Sutton, *Phys. Rev.* **128**, 591 (1962))

metal; the current is a flow of Cooper pairs and each Cooper pair responds to the vector potential averaged over its wavefunction.

★10.4.2 The Cooper problem

By solving a simple problem in 1956, Cooper provided the inspiration for the BCS theory. Cooper solved the Schrödinger equation for two interacting electrons in the presence of a Fermi sphere of non-interacting electrons, as shown in Fig. 10.12. This calculation cannot be applied directly to a real metal since it is impossible to turn off the interaction between all but two of the conducting electrons, but it serves to indicate the kind of effect that the interaction might produce. The wavefunction of the two electrons can be

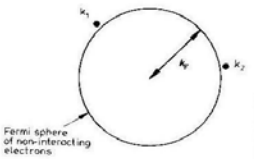

Fig. 10.12 The Cooper problem. Two interacting electrons are restricted to states, $\mathbf{k}_1$ and $\mathbf{k}_2$, outside the Fermi surface by the Fermi sphere of non-interacting electrons

expanded as a linear combination of plane waves (see Eq. (3.3))

$$\psi(\mathbf{r}_1, \mathbf{r}_2) = \sum_{\mathbf{k}_1} \sum_{\mathbf{k}_2} f(\mathbf{k}_1, \mathbf{k}_2) \, e^{i\mathbf{k}_1 \cdot \mathbf{r}_1} e^{i\mathbf{k}_2 \cdot \mathbf{r}_2} \quad (10.18)$$

where the role of the non-interacting electrons is to restrict the summation to plane wave states outside the Fermi sphere ($|\mathbf{k}_1|, |\mathbf{k}_2| > k_F$). Cooper looked for states of this form with an energy less than $2\varepsilon_F$, the energy of two 'normal' electrons at the Fermi surface. Such states would correspond to bound states of the two electrons and their existence would indicate that the normal state, as represented by the Fermi sphere, was unstable against the formation of bound pairs of electrons.

For the lowest energy, the centre of mass of the two electrons is at rest and this is achieved by including only states with equal and opposite momentum, $\mathbf{k}_1 = -\mathbf{k}_2 = \mathbf{k}$, in the expansion of Eq. (10.18), which then simplifies to

$$\psi(\mathbf{r}_1, \mathbf{r}_2) = \sum_{\mathbf{k}} g(\mathbf{k}) \, e^{i\mathbf{k} \cdot (\mathbf{r}_1 - \mathbf{r}_2)} \quad (10.19)$$

where the summation is again restricted to states $\mathbf{k}$ outside the Fermi surface. Cooper found that bound states existed if the interaction between the two electrons was attractive, no matter how weak the attraction; this was surprising in that bound states exist for two particles in a vacuum only if the attractive potential exceeds a threshold value. BCS made the bold extrapolation from Cooper's result that bound Cooper pairs would still result when all the electrons interacted with each other.

★10.4.3 Origin of the attractive interaction

An attractive interaction between electrons seems an unlikely possibility in view of the large repulsive force between two *isolated* electrons. We shall see in Chapter 13 however that the effective Coulomb interaction between two electrons in a metal is much reduced by the presence of the other electrons and the positive ions. Each electron repels other electrons from its neighbourhood and thereby creates a hole in the electron 'fluid' which is of order one atom in size and on average contains a positive charge from the ions equal and opposite to the electronic charge (Fig. 10.13(*a*)). The net charge in the neighbourhood of the electron is therefore approximately zero and the effective interaction of the electron with another electron outside the screening hole is weak.

The attractive force arises because an electron attracts the positive ions so that, as it moves through the metal, it leaves a wake of enhanced positive charge density behind it (Fig. 10.13(*a*)). Because ions move more slowly than electrons, the wake persists after the electron moves away and can attract another electron. The attraction is of very short range since the wake is only of the order of an atomic spacing in width, but it is retarded because the electron causing the wake

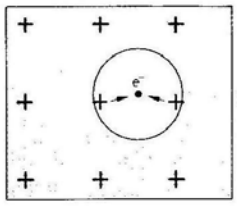

(*a*) Because of Coulomb repulsion an electron is surrounded by a screening hole in the electron fluid, which on average contains a positive charge equal and opposite to the electronic charge. The electron attracts the positively charged ion cores in its neighbourhood. The enhanced positive charge density persists after the electron moves away and can attract another electron

(*b*) The attractive interaction between two electrons can be pictured as the exchange of a virtual phonon. The phonon is virtual since an electron cannot undergo a sufficient energy change ($\sim \hbar\omega_D$) at low temperatures ($T \ll \theta_D$) to create a real phonon of short wavelength. A virtual phonon is emitted by one electron and absorbed by another within such a short time ($< 1/\omega_D$) that its 'existence' is allowed by the energy–time uncertainty relation. Momentum is conserved in the individual emission and absorption processes but energy is only conserved overall

Fig. 10.13

has already moved away. Since ionic motion communicates the interaction between the two electrons, the attraction is said to result from the exchange of virtual phonons (Fig. 10.13(*b*)). The detailed nature of the interaction is important in determining the transition temperature of the superconductor but the qualitative behaviour of the superconductor below T_c is determined almost entirely by the existence of the Cooper pairs. Indeed, BCS calculated successfully most of the properties of superconductors by replacing the real short-range retarded interaction by a fictitious but simpler instantaneous interaction spread out to a range $\sim v_F/\omega_D$ to allow for the distance moved by an electron during the characteristic time ($\sim 1/\omega_D$) for ionic motion.

★10.4.4 Nature of the superconducting ground state

According to the BCS theory all the electrons are paired at $T = 0$. Since the wavefunctions of all the pairs are identical, superconductivity is often described as arising because of a Bose condensation of Cooper pairs† (see Mandl,[2] p. 292). It is instructive to see how it is possible to write down a wavefunction that corresponds to such a ground state. The common wavefunction of all the pairs can be expanded in plane waves as in Eq. (10.19) except that the restriction to states with $|\mathbf{k}| > k_F$ is removed as there is now no non-interacting Fermi sphere. In most (perhaps all) known superconductors the pair wavefunction is essentially spherically symmetric, $\psi(\mathbf{r}_1, \mathbf{r}_2) = \psi(|\mathbf{r}_1 - \mathbf{r}_2|)$, so that the Cooper pair possess no orbital angular momentum; the spherical symmetry is distorted slightly by the anisotropy of the crystal structure but we will ignore this. The spherical symmetry corresponds to $g(\mathbf{k})$ depending only on the magnitude of $\mathbf{k}$ and the wavefunction is therefore symmetric under interchange of $\mathbf{r}_1$ and $\mathbf{r}_2$. An antisymmetric pair wavefunction $\phi(1, 2)$ can be obtained by combining this space wavefunction with the antisymmetric spin singlet wavefunction. Thus

$$\phi(1, 2) = \psi(|\mathbf{r}_1 - \mathbf{r}_2|)\frac{1}{\sqrt{2}}(\uparrow\downarrow - \downarrow\uparrow). \tag{10.20}$$

The electrons in the Cooper pair therefore have opposite spins. A wavefunction for N electrons which has $N/2$ pairs all in the same state can be written

$$\Psi(1, 2, 3, 4, \ldots, N) = P\{\phi(1, 2)\phi(3, 4)\ldots\phi(N-1, N)\} \tag{10.21}$$

where P is an operator that makes the product wavefunction in the curly brackets antisymmetric under interchange of any two electrons. We will not discuss how this is done in general but will demonstrate how it works for two pairs by writing down the wavefunction explicitly for this case:

$$\Psi(1, 2, 3, 4) = P\{\phi(1, 2)\phi(3, 4)\}$$

$$= \frac{1}{\sqrt{3}}[\phi(1, 2)\phi(3, 4) - \phi(1, 3)\phi(2, 4) - \phi(1, 4)\phi(3, 2)].$$

Eq. (10.21) is essentially the ground state wavefunction of the BCS theory.

In all superconductors where it has been possible to elucidate unambiguously the nature of the pairing, the Cooper pairs have been found to have zero orbital angular momentum. However, the nature of the pairing in high-temperature superconductors has not yet been established. Some heavy fermion superconductors‡ may also have finite angular momentum pairing. Liquid ^{3}He undergoes a superfluid transition due to Cooper pairing into a state with $L = 1$ and

† Although a tightly bound pair of fermions behaves like a boson, there are dangers in pushing this simple idea too far in the case of Cooper pairs; these are weakly bound and there is a strong overlap of the wavefunctions of neighbouring pairs.

‡ Heavy fermion materials such as UPt_3 and UBe_{13} are so called because they have a very large electronic heat capacity at low temperatures, equivalent to a large heat capacity effective mass for the electrons (section 3.2.3). This seems to arise because of a contribution to the density of states at the Fermi surface from the 5f electrons of the U atoms.

the neutrons in neutron stars are also believed to be in a Cooper paired state of finite angular momentum; these *neutral* Fermi systems cannot however be described as superconductors!

10.4.5 Explanation of infinite conductivity

To give a qualitative explanation of infinite conductivity we must first describe how it is possible to obtain a current-carrying state by giving all the pairs a finite centre-of-mass momentum. A uniform current density corresponds to a pair wavefunction of the form†

$$\phi = e^{i\mathbf{q}\cdot\mathbf{r}}\phi_0 \tag{10.22}$$

where $\mathbf{r} = (\mathbf{r}_1 + \mathbf{r}_2)/2$ is the centre-of-mass position of the two electrons and ϕ_0 is a wavefunction for a pair at rest. Eq. (10.22) corresponds to a centre-of-mass momentum $\hbar\mathbf{q}$ and hence to a velocity $\mathbf{v}$, where

$$\hbar\mathbf{q} = 2m\mathbf{v}.$$

As the charge on a Cooper pair is $-2e$ the resulting current density is

$$\mathbf{j} = -\frac{n_s}{2}2e\frac{\hbar\mathbf{q}}{2m} \tag{10.23}$$

for n_s superconducting electrons per unit volume ($n_s/2$ pairs).

Consider a wire carrying a Cooper pair current of this kind. We must explain why the scattering of electrons by phonons and impurities is ineffective in producing electrical resistance. The process in which a Cooper pair absorbs a phonon of energy of order $2\Delta(T)$ and two normal electrons are created (Fig. 10.14) undoubtedly occurs, as does the inverse process in which two normal electrons combine with the emission of a phonon to form a Cooper pair. Indeed these processes occur with equal rates in order to preserve a dynamic equilibrium between the concentrations of Cooper pairs and normal electrons.

Because the energy is lower when all the Cooper pairs are in the same state, the pairs created by phonon emission always have the wavefunction of Eq. (10.22); *unless their centre-of-mass motion is the same as that of the existing pairs, their binding energy vanishes*. The current is thus unaffected by phonon scattering. Since impurity scattering is elastic, impurities cannot scatter Cooper pairs at all; a change of momentum for a single Cooper pair involves the loss of its binding energy and is therefore an inelastic process. The pair current can only be changed by an influence that affects all the pairs equally such as an electric field.

† We assume a uniform current density for simplicity. Note that a spatially uniform current density can only be obtained in practice in a conductor (such as a thin film or fine wire) with one or more dimensions small compared to the penetration depth λ.

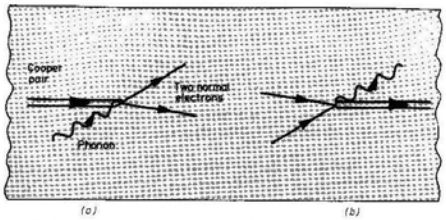

Fig. 10.14 Phonon scattering processes in a wire carrying a supercurrent: (*a*) absorption of a phonon by a Cooper pair of momentum $\mathbf{q}$ creates two normal electrons; (*b*) two normal electrons combine with the emission of a phonon to form a Cooper pair of momentum $\mathbf{q}$

10.5 MACROSCOPIC QUANTUM PHENOMENA

10.5.1 The superconducting order parameter

Since the Cooper pairs share a common wavefunction, the behaviour of the superconducting electrons is *completely* specified by this function; that a function of only two position variables is needed to describe $\sim 10^{29}$ electrons/m^3 is in complete contrast to the situation in a normal metal where the behaviour is only determined by specifying all of the single-particle states occupied. The coherence in the wavefunction associated with macroscopic occupation of the same quantum state by Cooper pairs causes superconductors to exhibit quantum mechanical effects on a macroscopic scale. A similar situation occurs for photons; the macroscopic occupation of a single quantum state leads to a macroscopically observable electric field.

For many purposes the relative motion of the two electrons in the pair can be ignored and the pair regarded as a point particle. Only the dependence of the wavefunction on the centre-of-mass coordinate needs to be considered and this is given by the **order parameter** $\psi(\mathbf{r})$;† thus, for example, we see from Eq. (10.22)

† Like the Weiss theory of ferromagnetism (section 8.3) the BCS theory is a mean field theory; the order parameter $\psi(\mathbf{r})$ is the mean field of the theory and is thus analogous to the magnetization of the ferromagnet. The mean field theory of superconductivity is more successful than that of ferromagnetism because fluctuation effects in macroscopic samples of superconductor occur so close to T_c that they are difficult to observe.

that the order parameter describing a state of uniform current density is

$$\psi(\mathbf{r}) = \psi_0 e^{i\mathbf{q}\cdot\mathbf{r}} \tag{10.24}$$

where A is a constant. Many of the properties of superconductors follow if $\psi(\mathbf{r})$ is regarded as the wavefunction of a particle of charge $-2e$ and mass $2m$ (appropriate to a Cooper pair).

The current density associated with such a wavefunction is given by making the substitutions $e \to 2e$, $m \to 2m$ in Eq. (C8) of appendix C:

$$\mathbf{j}(\mathbf{r}) = +\frac{i\hbar e}{2m}(\psi^*\nabla\psi - \psi\nabla\psi^*) - \frac{2e^2}{m}\psi^*\psi\mathbf{A}. \tag{10.25}$$

The most general form of $\psi(\mathbf{r})$ is

$$\psi(\mathbf{r}) = |\psi(\mathbf{r})|\, e^{i\theta(\mathbf{r})} \tag{10.26}$$

and inserting this in Eq. (10.25) we find

$$\mathbf{j}(\mathbf{r}) = -(e/m)|\psi(\mathbf{r})|^2(\hbar\nabla\theta + 2e\mathbf{A}). \tag{10.27}$$

This equation will be the starting point for our discussion of macroscopic quantum phenomena, but first we will use it to rederive two of our previous results:

(1) Inserting $\theta(\mathbf{r}) = \mathbf{q}.\mathbf{r}$ (Eq. (10.24)) and $\mathbf{A} = 0$ (see problem 10.8) into Eq. (10.27) gives Eq. (10.23) if the order parameter is normalized so that

$$|\psi(\mathbf{r})|^2 = n_s/2 = \text{Cooper pair density.}$$

(2) Taking the curl of Eq. (10.27) and assuming that the Cooper pair density $|\psi(\mathbf{r})|^2$ is independent of position (i.e. that the wavefunction is rigid) gives the London equation (10.9).†

10.5.2 Flux quantization

Far from the surface of a superconductor in its Meissner state we have $\mathbf{j} = 0$. Eq. (10.27) then becomes

$$\hbar\nabla\theta = -2e\mathbf{A}. \tag{10.28}$$

We integrate this equation around a closed curve C inside the superconductor,

$$\hbar\oint_C \nabla\theta.\mathrm{d}\mathbf{l} = \hbar\Delta\theta = -2e\oint_C \mathbf{A}.\mathrm{d}\mathbf{l}. \tag{10.29}$$

Since the order parameter $\psi(\mathbf{r})$ behaves like a wavefunction, it must be single-valued and the phase change $\Delta\theta$ around a closed loop must be $\pm 2\pi n$

† The price we pay for ignoring the internal structure of the Cooper pair wavefunction is to obtain the local London current–field relation rather than the true non-local relation. For an explanation of the difference between Eqs. (10.10) and (10.27) see problem 10.9.

where n is a positive (or zero) integer. The integral $\oint_C \mathbf{A}.\mathrm{d}\mathbf{l}$ may be transformed by Stokes' theorem as in Eq. (7.28) to show that it is equal to the magnetic flux Φ through the curve C. We thus obtain

$$\Phi = \pm\frac{2\pi n\hbar}{2e} = \pm\frac{nh}{2e} = \pm n\Phi_0, \tag{10.30}$$

which shows that the flux through any closed curve on which $\mathbf{j} = 0$ within a superconductor is quantized in units of the flux quantum $\Phi_0 = h/2e = 2.07 \times 10^{-15}\ \mathrm{T\,m^2}$.

Applying this result to the flux associated with the persistent current flowing around a superconducting ring (Fig. 10.15) we see that the current is also quantized and this sheds new light on its stability. A change in current corresponding to a change in flux through the ring of one quantum involves a change in $\Delta\theta$ of 2π. Such a change can only be achieved if the coherence of the superconducting wavefunction is temporarily destroyed in some way, with the consequent loss of condensation energy of the Cooper pairs. There is thus a large energy barrier against such a change. Because of the energy associated with the current and the trapped flux, a state with a finite persistent current is strictly only metastable, but with an effectively infinite lifetime.

Fig. 10.16 illustrates schematically an experiment that used a superconducting ring to measure the flux quantum. The specimen was in the form of a thin film of tin electroplated onto a fine copper wire a few millimetres long and about 10 μm diameter (remember that copper is an insulator in comparison with superconductors!); the small diameter was used so that one flux quantum corresponded to a reasonable field ($\sim 10\ \mu$T) within the ring. The sample was placed in a magnetic field of this order and cooled through the transition temperature; the field was then removed and the trapped flux measured by vibrating the sample between two search coils connected in series opposition. The experiment was repeated a number of times and the trapped flux as a function of the initial

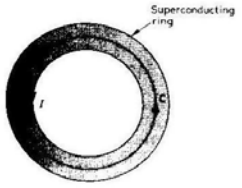

Fig. 10.15 Integration of Eq. (10.28) round the curve C proves that the magnetic flux through the superconducting ring is quantized. The persistent current I that gives rise to the flux flows on the inner surface of the ring

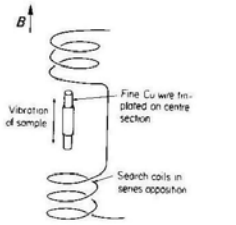

(*a*) Experimental arrangement for measuring the flux quantum

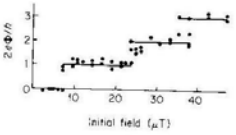

(*b*) Flux trapped in the ring after it had been cooled through the superconducting transition in a magnetic field, which was then removed. (Reproduced with permission from B. S. Deaver and W. M. Fairbank, *Phys. Rev. Lett.* 7, 43 (1961))

Fig. 10.16

applied field is shown in Fig. 10.16(*b*). Quantization in units of $h/2e$ is apparent; the number of quanta is such as to make the trapped field as close as possible to the initial applied field. The higher quanta in Fig. 10.16(*b*) become less well defined probably because of a flaw in the tin film part way along its length through which one or more flux quanta could pass.

The magnitude of the flux quantum provides very strong evidence of the presence of Cooper pairing in superconductors. The factor 2 in the denominator of $h/2e$ comes from the 2 in the second term in brackets in Eq. (10.27), and thus directly from the charge on a Cooper pair. We should reassure the reader worried about the lack of rigour in our derivation of flux quantization (for example in our neglect of the internal structure of the Cooper pair wavefunction) that a rigorous derivation can be given, based only on the symmetry properties of the order parameter.

10.5.3 Quantized flux lines and type II superconductivity

We next consider the implications of flux quantization through a curve C surrounding a region completely filled by superconductor. We suppose that one

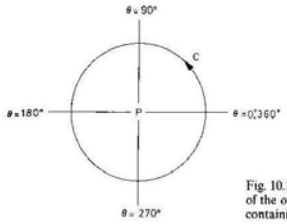

Fig. 10.17 Contours of constant phase of the order parameter for a curve C containing one quantum of magnetic flux

flux quantum passes through C so that the phase θ of the superconducting order parameter changes by 2π in one complete circuit of C. Contours of constant phase could then appear as in Fig. 10.17 and this creates a problem at a point P within C where θ must take on all values between 0 and 2π simultaneously. As this is inconsistent with the requirement of a single-valued order parameter it would appear to rule out the passage of quantized magnetic flux through the interior of a superconductor, thereby implying that the superconductor is in the Meissner state.

There is an alternative possibility. If we allow $|\psi|$ to go to zero at point P, then the order parameter is again single-valued there (the single value is zero); the phase of the order parameter is undefined at a point where $|\psi| = 0$. If we repeat this argument for other sections through the superconductor then we find that $|\psi|$ must vanish along a continuous line and we are thus led to the concept of a **quantized flux line**. The structure of such a line is shown in Fig. 10.18. The density of Cooper pairs $|\psi|^2$ falls to zero on the line (Fig. 10.18(*a*)), which can therefore be pictured as a filament of non-superconducting material. There is a circulating current around the line (Fig. 10.18(*b*)), which generates the magnetic field (Fig. 10.18(*c*)) associated with the quantized flux.

An array of quantized flux lines provides the mechanism for the flux penetration in the mixed state of type II superconductors (section 10.2.3); electron microscopy studies† indicate that the flux lines tend to form a regular triangular lattice. In principle it is possible to have lines containing more than one quantum of flux but they would have a higher energy and only singly quantized lines are found in practice. We see from Fig. 10.18 that there are two length scales associated with a flux line. From section 10.3 we expect the length scale for the current and field variation (Figs. 10.18(*b*) and (*c*)) to be the penetration depth λ. We might expect the length scale ξ for the variation of $|\psi|^2$

† See, for example, U. Essman and H. Träuble, *Scientific American*, **224** (March), 74 (1971)).

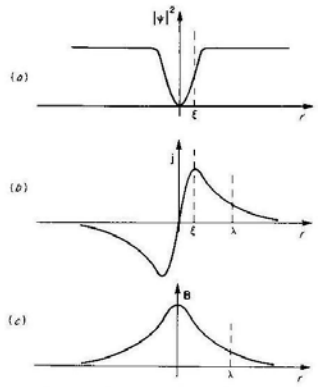

Fig. 10.18 Variation of $|\psi|^2$, j and B through a quantized flux line

(Fig. 10.18(*a*)) to be associated with the size of the Cooper pair wavefunction; this indeed turns out to be the case and in a pure superconductor

$$\xi \approx \frac{\xi_0}{(1 - T/T_c)^{1/2}} \tag{10.31}$$

where ξ_0 is the BCS coherence length of Eq. (10.17).

We can now answer qualitatively the question of why some superconductors are type I and others type II by estimating the energy cost of forming a plane boundary between a superconducting and normal region in a type I superconductor as shown in Fig. 10.19; since the superconducting and normal phases are in equilibrium at the applied field B_c the free energies per unit volume of the bulk uniform regions on either side of the boundary are equal. In the boundary region itself however there is a loss of condensation energy over a distance ξ at the boundary, resulting in an *increase* in free energy

$$\Delta G_C \approx (G_N - G_S)\xi \tag{10.32}$$

per unit area of boundary, where $G_N - G_S$ is the condensation energy per unit volume. The presence of the boundary allows the field B_c to penetrate the

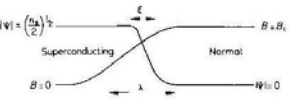

Fig. 10.19 Boundary between a normal and superconducting region in a type I superconductor. The boundary can only be in equilibrium at an applied field B_c. The order parameter decays in a distance of order ζ and the field penetrates a distance of order λ into the superconducting region

superconducting region a distance of order λ, resulting in a *decrease* in free energy

$$\Delta G_B \approx -\frac{1}{2\mu_0} B_c^2 \lambda \tag{10.33}$$

per unit area of boundary. We expect type I behaviour only if the energy associated with the formation of the boundary, $\Delta G_C + \Delta G_B$, is positive. From Eq. (10.6), $(G_N - G_S)$ and $B_c^2/2\mu_0$ are equal, so that the condition for type I behaviour is approximately $\xi > \lambda$. When $\xi < \lambda$ it is energetically favourable for the superconductor in an applied field of order B_c to break up into a mixture of normal and superconducting regions; the energy decrease associated with the penetration of the field into the superconducting regions more than compensates for the loss of condensation energy. The arrangement of normal and superconducting regions with the lowest energy is the lattice of quantized flux lines; if $\xi < \lambda$ type II behaviour is therefore expected. When the mean free path of the electrons is decreased, λ increases and ξ decreases, and this explains the change in behaviour from type I to type II that is produced by alloying in many metals.

The existence of superconductivity up to fields of order 40 T in some type II alloys and compounds (Fig. 10.8) explains the use of these materials in the construction of solenoids for the generation of large magnetic fields. The major problem is to find materials that will carry a large dissipationless current in high fields. To explain the problem we consider a solenoid with its ends connected together to form a continuous superconducting circuit; the field is generated by a persistent current flowing in this circuit. In type II superconductors such a field can unfortunately decay by the passage of quantized flux lines across the windings and out of the coil and this is equivalent to the coil having a finite electrical resistance. Some mechanism is required to prevent the free migration of flux lines. This is usually done by making the material inhomogeneous, either by precipitation or work hardening; regions where the flux line energy is low are thereby produced and these act as **pinning centres** for the flux lines. Such

materials are characterized by highly irreversible magnetization curves. High-temperature superconductors have even larger values of B_{c2} than the materials shown in Fig. 10.8 but the problem of flux pinning at liquid nitrogen temperatures has yet to be solved in these materials.

Another important problem in superconducting solenoids is the possibility that a small region may revert to the normal state, which has a high resistivity. The consequent heating rapidly causes the whole magnet to become normal; the energy stored in the magnetic field is dumped in the liquid helium bath with disastrous consequences. In practice the superconducting wire is a composite of superconductor and copper, such that, if a small region does become normal, the copper carries the current with little dissipation, thus preventing rapid growth of the normal region.

10.5.4 Josephson effects

Josephson effects are probably the most striking manifestation of macroscopic quantum phenomena. They occur when two macroscopic superconducting regions are **weakly coupled**. To explain what this means we consider first two isolated samples of a superconductor with spatially constant order parameters $|\psi_1| \exp(i\theta_1)$ and $|\psi_2| \exp(i\theta_2)$ as shown in Fig. 10.20(*a*). If the temperature of both samples is the same then

$$|\psi_1|^2 = |\psi_2|^2 = n_s/2.$$

In the absence of interaction between the two samples however the phases θ_1 and θ_2 will in general be different; all that is required is that the phase should be spatially constant within each region corresponding to the Cooper pairs being at rest. Strongly coupling the two samples by bringing them into contact over a large area causes the phase to equalize, $\theta_1 = \theta_2$, so that all the Cooper pairs can be in the same state; this equality is then very difficult to disturb. If there is weak coupling, the lowest energy state is still one with $\theta_1 = \theta_2$, but it is possible to generate a phase difference between the two regions by passing a small current though the coupling or applying a small voltage across it. Two superconductors, weakly coupled in this sense, are said to form a **Josephson junction**; the coupling between them is decribed as a **weak link**.

There is more than one way of achieving weak coupling but we will restrict our discussion to two superconductors separated by an oxide barrier of a few atoms thickness as shown in Fig. 10.20(*b*); the coupling arises because electrons can cross the barrier by a quantum mechanical tunnelling process. When the metal is in its normal state the tunnelling current through the barrier is proportional to the voltage across it; such behaviour is described as **ohmic** and a typical junction resistance is 1 Ω.

Below T_c it is possible for Cooper pairs to tunnel through the oxide barrier; a net flow can take place in the absence of an applied potential difference and this

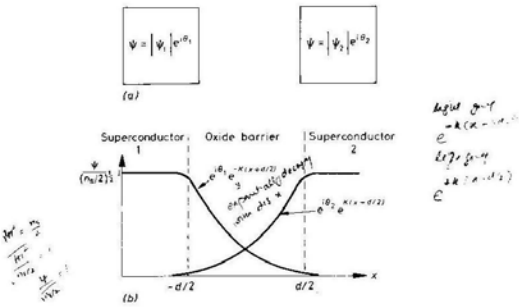

Fig. 10.20 (*a*) Two isolated samples of a superconductor. (*b*) The contributions to the superconducting order parameter within the oxide barrier associated with the tunnelling of Cooper pairs through the barrier

corresponds to a dissipationless supercurrent, which we now calculate. Because of the tunnelling of the pairs, the superconducting order parameter extends throughout the barrier; inside the barrier we regard it as being the sum of the contributions shown in Fig. 10.20(*b*): one contribution originates in region 1 and decays exponentially within the barrier, and the other originates in region 2 and decays within the barrier. We assume that the contribution from region 1 is very small by the time it reaches region 2 and vice versa so that we can regard the order parameter within the superconducting region as retaining its 'bulk' value up to the edge of the barrier. We therefore write the order parameter within the barrier as

$$\psi = (n_s/2)^{1/2}(e^{i\theta_1 - K(x + d/2)} + e^{i\theta_2 + K(x - d/2)}) \tag{10.34}$$

where the barrier extends from $x = -d/2$ to $x = d/2$ and K^{-1} is the characteristic length for decay of the order parameter within the barrier. θ_1 and θ_2 are the phases of the order parameter on the two sides of the junction. To calculate the pair current density through the barrier we use Eq. (10.25) with $\mathbf{A} = 0$ and the order parameter of Eq. (10.34) to find

$$j = \frac{ie\hbar n_s}{2m} K e^{-Kd}(-e^{i(\theta_1 - \theta_2)} + e^{i(\theta_2 - \theta_1)}) = j_0 \sin\delta, \tag{10.35}$$

where $\delta = \theta_1 - \theta_2$ is the phase difference between the two sides of the junction and $j_0 = ehn_S K \exp(-Kd)/m$.

If a current is caused to flow through the junction the phase difference adjusts itself so that the **Josephson equation** (10.35) is satisfied. The existence of dissipationless flow of Cooper pairs through a weak link is called the **dc Josephson effect** and experimental confirmation of this effect is seen in Fig. 10.21. The maximum current density in the oxide barrier is j_0, corresponding to a phase difference δ of $\pi/2$. What happens when this current is exceeded depends on the load line of the circuit used to provide the current; the behaviour for the circuit used to obtain the results of Fig. 10.21 is indicated in the figure.

The current observed at finite voltages in Fig. 10.21 coresponds to tunnelling of normal electrons through the oxide barrier. At low temperatures where all the electrons on both sides of the barrier are paired, the tunnelling of a normal electron requires the breaking of a pair. This can only occur if the electron tunnelling through the barrier gains an energy 2Δ from the voltage difference across the barrier. The current is therefore small until the voltage reaches a value $2\Delta(T)/e$. The increase in current when this condition is satisfied is apparent on Fig. 10.21 and normal electron tunnelling provides an accurate and direct method for measuring $\Delta(T)$; the measurements of Fig. 10.11 were obtained by this method. At voltages above $2\Delta(T)/e$ the current–voltage relation reverts to the ohmic behaviour characteristic of the normal state.

What happens to the Cooper pair tunnelling at finite voltages? To answer this question we must consider the time dependence of the superconducting order parameter. Since the order parameter acts as the wavefunction of the Cooper

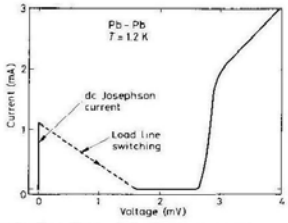

Fig. 10.21 Current voltage characteristic of a Pb–PbO–Pb tunnel junction at 1.2 K. The current spike at $V = 0$ is the dc Josephson effect. (Reproduced with permission from D. N. Langenburg *et al., Proc. IEEE* **54**, 560 (1966). © 1966 IEEE)

pairs we might expect a dependence of the form

$$\psi \propto e^{-i\mu t/\hbar},$$

where μ is the energy of a pair; the relevant energy turns out to be the chemical potential of the pair. More generally if μ depends on time we have

$$\psi \propto e^{i\theta(t)}$$

where

$$\hbar\, \partial\theta/\partial t = -\mu. \tag{10.36}$$

Ordinarily, because a superconductor cannot sustain a potential difference, μ is uniform and Eq. (10.36) has no observable consequences. It is however possible to maintain a potential difference V between two weakly coupled superconductors, in which case we deduce from Eq. (10.36) that

$$\hbar \frac{\partial \theta_1}{\partial t} - \hbar \frac{\partial \theta_2}{\partial t} = -\mu_1 + \mu_2 = 2eV$$

or

$$\hbar \frac{\partial \delta}{\partial t} = 2eV \tag{10.37}$$

where δ is the phase difference across the junction as in Eq. (10.35).

If V is a constant we can integrate Eq. (10.37) to obtain

$$\delta = \frac{2eV}{\hbar} t + \delta_0 \tag{10.38}$$

where δ_0 is the value of δ at $t = 0$. The phase difference thus increases linearly with time and inserting this in Eq. (10.35) for the current gives

$$j = j_0 \sin\left(\frac{2eV}{\hbar} t + \delta_0\right). \tag{10.39}$$

At finite potential difference therefore there is an ac supercurrent of Cooper pairs at a frequency $\nu = \omega/2\pi = 2eV/h$ and this is known as the **ac Josephson effect**; because the current is alternating it is not seen in the dc current–voltage characteristic of Fig. 10.21. The ratio of the voltage to the frequency is $h/2e$ = the flux quantum = 2.07×10^{-15} V Hz^{-1}, and the ac Josephson effect provides a very accurate method of measuring this ratio of fundamental constants.

One way of observing the ac Josephson effect is to irradiate the junction with microwaves of frequency ω in addition to applying a dc potential V_0. The total potential difference is then $V_0 + v\cos(\omega t)$ and integrating Eq. (10.37) gives

$$\delta = \frac{2e}{\hbar}\left(V_0 t + \frac{v}{\omega}\sin(\omega t)\right) + \delta_0.$$

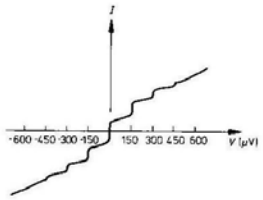

Fig. 10.22 Steps induced on the current–voltage relation of a point-contact Josephson junction by microwave radiation of frequency 72 GHz. The junction is formed by contact between a sharply pointed piece of niobium and a flat niobium surface. (Reproduced with permission from C. C. Grimes and S. Shapiro, *Phys. Rev.* **169**, 397 (1968))

The resulting pair current through the junction, from Eq. (10.35), is

$$j = j_0 \sin\left[\frac{2e}{\hbar}\left(V_0 t + \frac{v}{\omega}\sin(\omega t)\right) + \delta_0\right]$$

which is a frequency-modulated current containing components at frequencies $(2e/\hbar)V_0 \pm n\omega$, where n is any integer. Thus there is a dc current (zero frequency) if

$$V_0 = \frac{n\hbar\omega}{2e}. \tag{10.40}$$

Fig. 10.22 shows the current–voltage characteristic of a microwave-irradiated Josephson junction, which shows well defined steps at the voltages predicted by Eq. (10.40). It is the steepness of the steps that enables $h/2e$ to be determined with precision† (see W. H. Parker, *et al., Phys. Rev.* **177**, 639 (1969)).

★10.5.5 Quantum interference

Consider a superconductor ring containing two identical Josephson junctions, labelled a and b, as shown in Fig. 10.23(*a*). From Eq. (10.35) the current I flowing through the junctions in parallel is

$$I = Aj_0 \sin\delta_a + Aj_0 \sin\delta_b = 2Aj_0 \cos\left(\frac{\delta_a - \delta_b}{2}\right)\sin\left(\frac{\delta_a + \delta_b}{2}\right) \tag{10.41}$$

where δ_a and δ_b are the phase differences across junctions a and b respectively and A is the area of each junction. We now show that $\delta_a - \delta_b$ is determined by

† The position of the steps can be determined with such great precision that the accuracy of the $h/2e$ measurement is limited by the accuracy with which standard voltage sources can be calibrated. This has led to the use of the Josephson junction as a means of establishing a voltage standard by *defining* a value of $h/2e$; the defined value is of course consistent with the best known value of this ratio.

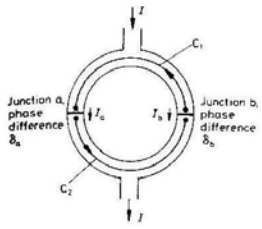

(*a*) Current flow through two Josephson junctions, a and b, in parallel

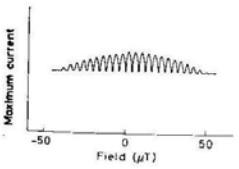

(*b*) Maximum current passed by the junctions as a function of applied magnetic field. The amplitude of the variation falls off at higher fields because the field causes the phase difference within each junction to vary with position. (Reproduced with permission from R. C. Jaklevic *et al., Phys. Rev.* **140**, A1628 (1965))

Fig. 10.23

the magnetic flux through the ring. We use an approach similar to that used to prove flux quantization in section 10.5.2. Because the current density vanishes along the curves C_1 and C_2 in the bulk superconducting regions, Eq. (10.28) is valid and integrating this along these curves we find

$$\theta_{a1} - \theta_{b1} = \frac{2e}{\hbar}\int_{C_1} \mathbf{A}.\mathbf{dl} \qquad \text{and} \qquad \theta_{b2} - \theta_{a2} = \frac{2e}{\hbar}\int_{C_2} \mathbf{A}.\mathbf{dl},$$

where θ_{a1}, θ_{b1}, θ_{a2} and θ_{b2} are the phases are at the ends of curves C_1 and C_2 close to the junctions indicated by the subscripts. Adding these equations gives

$$\delta_a - \delta_b = \frac{2e}{\hbar}\oint_C \mathbf{A}.\mathbf{dl} = \frac{2e\Phi}{\hbar}. \tag{10.42}$$

where Φ is the flux through the ring and $\delta_a = \theta_{a1} - \theta_{a2}$ and $\delta_b = \theta_{b1} - \theta_{b2}$ are phase differences across the two junctions. In order to obtain the integral of round a closed curve we have had to include the small contributions from the

junctions themselves; this introduces negligible error since A varies smoothly through the very narrow junction region.

Inserting Eq. (10.42) into Eq. (10.41) gives

$$I = 2AJ_0 \cos\left(\frac{e}{\hbar}\Phi\right) \sin\left(\frac{\delta_a + \delta_b}{2}\right). \tag{10.43}$$

This resembles the supercurrent (Eq. (10.35)) through a single junction; for the double junction it is $(\delta_a + \delta_b)/2$ that varies to match the current I fed into the ring. The maximum supercurrent that the junction can carry is now

$$I_{max} = 2AJ_0 \left|\cos\left(\frac{e}{\hbar}\Phi\right)\right| \tag{10.44}$$

and thus varies periodically with Φ; the period is just the flux quantum $\hbar/2e$. The measured variation of maximum supercurrent for a double junction can be seen in Fig. 10.23(*b*). If the two junctions are not identical then the maximum current varies periodically with Φ but does not fall to zero as predicted by Eq. (10.44).

We designate this effect **quantum interference** because of the analogy with the Young's slits interference experiment in optics (Smith and Thomson,[5] p. 127). The difference $\delta_a - \delta_b$ is analogous to the phase difference between the rays of light from the slits to the screen on which the interference pattern is observed; Eq. (10.44) thus corresponds to the cosine dependence of the light amplitude with position on the screen. Experiments with superconducting interferometers have been performed with junctions separated by distances of order 1 cm, impressive evidence that the superconducting order parameter is phase coherent over truly macroscopic distances.

Because of the smallness of the flux quantum, a pair of junctions as in Fig. 10.23(*a*) embracing an area of 1 cm^2 would change from maximum to minimum critical current for a change of field of only 10^{-11} T. The dc SQUID (superconducting quantum interference device) is an instrument that exploits this geometry to measure very small magnetic fields with great precision.

10.6 HIGH-TEMPERATURE SUPERCONDUCTORS

High-T_c superconductors are all oxides and have many other features in common. We use the widely studied $YBa_2Cu_3O_{7-\delta}$ to illustrate their behaviour; this material has $T_c = 92$ K and is referred to as a 1-2-3 superconductor because of the relative numbers of metal atoms in its chemical formula. The yttrium can be replaced by various other trivalent atoms (e.g. holmium and neodymium) without any significant effect on the superconducting properties. The crystal structure of $YBa_2Cu_3O_{7-\delta}$ is shown in Fig. 10.24(*a*). It contains planes of Cu and O atoms with the chemical formula CuO_2 as indicated; all superconductors with a T_c greater than 50 K discovered up to 1990 possess CuO_2 (or NiO_2)

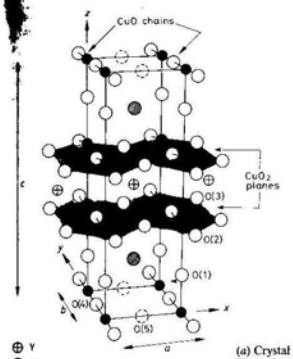

(*a*) Crystal structure of $YBa_2Cu_3O_{7-\delta}$. The unit cell is as indicated. Five different oxygen sites are identified; for $\delta \approx 0.1$ the O(4) sites are almost full and the O(5) sites empty

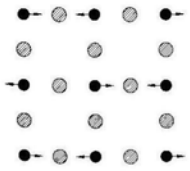

(*b*) Plan of CuO_2 plane showing antiferromagnetic arrangement of Cu spins that occurs for δ greater than about 0.6

Fig. 10.24

planes similar to these and it is believed that they play a crucial role in the conductivity and superconductivity of high-T_c superconductors. $YBa_2Cu_3O_{7-\delta}$ also has chains of alternate Cu and O atoms as identified in Fig. 10.24(*a*).

The electrical resistivity of $YBa_2Cu_3O_{7-\delta}$ in its normal state is very anisotropic, being much higher for current flow along the z axis than for current flow in the xy plane. This is normally regarded as evidence that conduction is predominantly due to motion of carriers in the CuO_2 planes. Discussion of the behaviour of $YBa_2Cu_3O_{7-\delta}$ is often simplified by regarding each CuO_2 plane as an isolated two-dimensional system. When we do this the reader should remember that this is a gross oversimplification; a complete understanding of the properties of $YBa_2Cu_3O_{7-\delta}$ can only be obtained by taking into account its complicated three-dimensional structure.

It is instructive to consider what happens as the amount of oxygen in $YBa_2Cu_3O_{7-\delta}$ is varied. We start with $YBa_2Cu_3O_6$, corresponding to $\delta = 1$. In this material the oxygen atoms in the CuO chains in Fig. 10.24(*a*) are completely absent. Since there is then nothing to distinguish the x direction from the y direction the structure is tetragonal ($a = b \neq c$, $\alpha = \beta = \gamma = 90°$). $YBa_2Cu_3O_6$ is an electrical insulator; in this material the CuO_2 plane can be considered approximately as being made of Cu^{2+} and O^{2-} ions. The Cu^{2+} ions have nine 3d electrons in their outer shell with a total spin $S = \frac{1}{2}$.† The Cu spins order antiferromagnetically, as shown in Fig. 10.24(*b*), with a Néel temperature just above 400 K. The O^{2-} ions have a filled 2p outer shell and therefore no magnetic properties.

When oxygen is added to $YBa_2Cu_3O_6$, the additional atoms initially occupy the sites marked O(4) and O(5) on Fig. 10.24(*a*) randomly; the structure therefore remains tetragonal. The added oxygen atoms act like acceptor impurities in a semiconductor (section 5.3) and thus add holes to the crystal. Some of these holes are located on the CuO_2 planes but for small concentrations there is no conduction; $YBa_2Cu_3O_{7-\delta}$ remains an antiferromagnetic insulator until δ decreases to about 0.6. This can be understood by assuming that the holes are localized on oxygen atoms in the CuO_2 planes. An oxygen atom with a hole has an outer shell with five 2p electrons and thus spin $S = \frac{1}{2}$. The localization of the holes is an indication that electron–electron interactions are important in the CuO_2 layers (see sections 4.3.2 and 13.5.6).

When the additional oxygen corresponds to a reduction in δ to about 0.6 two important changes occur: the symmetry of the crystal structure changes from tetragonal to orthorhombic ($a \neq b \neq c$, $\alpha = \beta = \gamma = 90°$) and an insulator–metal transition occurs (section 13.5.6). The extent to which these changes are related is not yet known. The change in crystal structure is due to preferential occupation of the O(4) sites over the O(5) sites, thus breaking the x–y symmetry

† This follows form Hund's rules (section 7.2.1). Presumably the orbital angular momentum of the ion is quenched by the crystal field.

and leading to the formation of the CuO chains in Fig. 10.24(*a*). The onset of conduction is due to delocalization of the holes; it is not clear if it is better to view the conduction as arising because of the hopping of a hole from one oxygen atom to another or as being linked with the formation of a two-dimensional energy band associated with the hybridization (section 4.3.4) of 3d states on the Cu atoms with 2p states on the oxygen atoms.

For δ just less than 0.6 the metallic $YBa_2Cu_3O_{7-\delta}$ undergoes a superconducting transition at about 40 K, but as δ decreases further T_c increases and reaches 92 K at $\delta \sim 0.1$. It has proved impossible to prepare $YBa_2Cu_3O_{7-\delta}$ with the structure shown in Fig. 10.24(*a*) with values of δ any smaller than about 0.1. The superconductivity is interpreted as arising because of Cooper pairing of the holes; flux quantum measurements indicate that pairing of particles with a charge of magnitude e is involved. The interaction responsible for pair formation has not yet been identified; the binding energy of the pairs is rather too high to be explained only by the mechanism involving the lattice vibrations that is responsible for Cooper pairing in 'conventional' superconductors. The antiferromagnetic order of the Cu atoms disappears at the insulator–metal transition but it is possible that the antiferromagnetic interactions between the Cu spins may play a role in the superconducting transition.

Our discussion would suggest that the superconductivity of $YBa_2Cu_3O_{7-\delta}$ is essentially two-dimensional. In practice this means that the properties of $YBa_2Cu_3O_{7-\delta}$ are very anisotropic. The critical current, for example, is much larger for flow of current in the xy plane than for flow along z. The high T_c and small Fermi velocity of $YBa_2Cu_3O_{7-\delta}$ mean that the coherence length (Eq. (10.17)), which measures the size of the Cooper pair wavefunction, is small, comparable to the size of the unit cell. In contrast the low carrier density implies through Eq. (10.14) that the penetration depth is large. The high-T_c superconductors are therefore extreme type II with very large values of B_{c2}.

Because of this and the fact that they are superconducting at the temperature of liquid nitrogen (77 K) there are many potential applications for these materials.† Difficult problems must however be overcome before the materials come into widespread use. Paramount among the problems for $YBa_2Cu_3O_{7-\delta}$ is that it is most easily prepared as a ceramic, that is as many small crystallites bonded together. Although the critical current parallel to the xy plane within each crystallite is high, the performance of the ceramic is degraded by poor contact between crystallites; it is possible to improve this by aligning the crystallites so that the xy planes in neighbouring crystallites are parallel. If the materials are to carry large currents in high magnetic fields some means of pinning the quantized flux lines must be devised. This problem is more acute in high-T_c superconductors operating at liquid nitrogen temperature because more

† See 'The new superconductors: prospects for applications' by A. M. Wolsky, R. F. Geise and E. Daniels, in *Scientific American*, February 1989.

thermal energy is available to allow the flux line to escape from its pinning centre.

PROBLEMS 10

10.1 A current is induced to flow around the walls of the thin lead tube shown at 4.2 K (not to scale, all dimensions in cm):

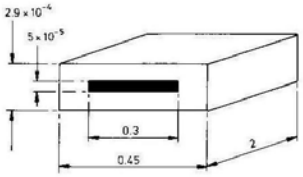

The current decays by less than 2% (the experimental sensitivity) in a time of 7 h. Deduce an upper limit for the electrical resistivity of superconducting lead. Assume a value 5×10^{-8} m for the penetration depth of lead. (This problem is based on the experiment of Quinn and Ittner, *J. Appl. Phys.* **33**, 748 (1962).)

10.2 The superconductor tin has $T_c = 3.7$ K and $B_c = 30.6$ mT at $T = 0$. Calculate the critical current for a tin wire of diameter 1 mm at $T = 2$ K. What diameter of wire would be required to carry a current of 100 A?

10.3 Use the approximate form of Eq. (10.1) for B_c to deduce approximate temperature dependences for the differences of the free energy, entropy and heat capacity between the normal and superconducting states. What is the discontinuity in the heat capacity at the superconducting transition in zero applied field?

10.4 Show that the Clogston limiting value of B_{c2} for a type II superconductor is given by $\mu_B B_{c2} \approx k_B T_c$.

10.5 Use the London equation to show that the penetration of a parallel magnetic field into a superconducting film of thickness d in the xy plane is described by

$$B = B_a \cosh(z/\lambda)/\cosh(d/2\lambda)$$

where B_a is the applied field and the centre of the film is at $z = 0$. Calculate the field at which the Gibbs free energies of the normal and superconducting states are equal for the film.

10.6 The effect of the non-locality of the current–field relation on the zero-temperature penetration depth of a pure type I superconductor in the limit $\lambda \ll \xi$ may be estimated by saying that, as the field decays on a length scale λ but the current depends on the average of $\mathbf{A}$ over a length scale ξ, the effective value of $\mathbf{A}$ to insert in Eq. (10.10) is $\lambda\mathbf{A}/\xi$. Show that this approach predicts

$$\lambda^3 = \lambda_L^2(0)\xi.$$

(The exact result from the BCS theory is $\lambda^3 = 0.62\lambda_L^2(0)\xi_0$.)

10.7 Suggest reasons for the following:
(*a*) At $T = 1$ K tin strongly absorbs electromagnetic radiation of wavelength 0.9 mm but only weakly absorbs radiation of wavelength 1.1 mm.
(*b*) Superconductors are poor conductors of heat for $T \ll T_c$.
(*c*) The critical field at $T = 0$ of different superconductors is *approximately* proportional to T_c.
(*d*) For different isotopes of the same element T_c depends on the isotopic mass.

10.8 A supercurrent, corresponding to the order parameter $(n_s/2)^{1/2} \exp(iqx)$, flows in a thin film in the xy plane of thickness $d \ll \lambda$. Calculate the vector potential within the film in a gauge for which $\mathbf{A} = 0$ in the centre of the film and $\operatorname{div} \mathbf{A} = 0$. Show that in this gauge the second term in Eq. (10.27) is smaller by a factor $\sim d^2/\lambda_L^2(T)$ than the first term.

10.9 Eq. (10.10) cannot be generally valid since the left-hand side must be invariant under a gauge change $\mathbf{A} \to \mathbf{A} + \nabla\chi$ of the vector potential whereas the right-hand side obviously is not (both A's give the same field $\mathbf{B}$). The correct gauge-invariant equation is Eq. (10.27). Explain why the gauge in which Eq. (10.10) is valid satisfies $\operatorname{div} \mathbf{A} = 0$. Use Eq. (10.27) to deduce the change in the order parameter due to the gauge transformation $\mathbf{A} \to \mathbf{A} + \nabla\chi$.

10.10 Deduce:
(*a*) the condensation energy, $G_N - G_S$, of lead from Fig. 10.4;
(*b*) dB_c/dT at T_c for aluminium (molar volume 10^{-5} m^3) from Fig. 10.6;
(*c*) the cross-sectional area of the tin cylinder from Fig. 10.16(*b*);
(*d*) the energy gap of lead from Fig. 10.21;
(*e*) the flux quantum from Fig. 10.22;
(*f*) the area of the loop containing the double junction from Fig. 10.23(*b*).